Hindawi
Journal of Analytical Methods in Chemistry
Volume 2021, Article ID 6670913, 10 pages
https://doi.org/10.1155/2021/6670913

Research Article

Graphene Oxide/Polyvinyl Alcohol/Fe_3O_4 Nanocomposite: An Efficient Adsorbent for Co(II) Ion Removal

Thu Dieu Le, Luyen Thi Tran, Hue Thi Minh Dang, Thi Thu Huyen Tran, and Hoang Vinh Tran

School of Chemical Engineering, Hanoi University of Science and Technology, 1 Dai Co Viet Road, Hanoi, Vietnam

Correspondence should be addressed to Hoang Vinh Tran; hoang.tranvinh@hust.edu.vn

Received 19 December 2020; Revised 3 February 2021; Accepted 26 February 2021; Published 9 March 2021

Academic Editor: Dang Quoc Thuyet

In this work, an effective nanocomposite-based adsorbent directed to adsorb cobalt (Co^{2+}) ion was successfully synthesized from graphene oxide (GO), polyvinyl alcohol (PVA), and magnetite (Fe_3O_4) nanoparticles via a coprecipitation technique. The synthesized GO/PVA/Fe_3O_4 nanocomposite was applied for Co^{2+} ion removal with the optimized working conditions including 100 min of contact time, 0.01 g of adsorbent dosage, pH of 5.2, and 50°C of temperature. The investigation of adsorption kinetics showed that the adsorption of Co^{2+} ion onto the GO/PVA/Fe_3O_4 nanocomposite followed the pseudo-second-order kinetic model with the rate constant k_2 being 0.0026 ($g\,mg^{-1}\cdot min^{-1}$). The Langmuir model is suitable to describe the adsorption of Co^{2+} ion onto the GO/PVA/Fe_3O_4 nanocomposite with the maximum sorption capacity (q_{max}) reaching 373.37 $mg\cdot g^{-1}$. The obtained results also indicated that the GO/PVA/Fe_3O_4 nanocomposite can adsorb/regenerate for at least 5 cycles with a little reduction in removal efficiency. Therefore, we believe that the GO/PVA/Fe_3O_4 nanocomposite could be used as a potential adsorbent for heavy metal treatment in terms of high adsorption capacity, fast adsorption rate, and recyclability.

1. Introduction

Nowadays, electronic devices are becoming more and more common in our life, in which rechargeable batteries are an indispensable item in every family and for every individual. However, the reality indicates that the manufacturing of rechargeable batteries, electrodes, gas turbine engines, hard permanent magnets etc. use a huge amount of cobalt (Co) and discharge a lot of cobalt ions (Co^{2+}) into the environment. Inhalation of Co dust may cause adverse respiratory effects, also causing neurological symptoms and cancer in human beings with unknown mechanism [1–3]. Therefore, there are many kinds of technologies to reduce the concentration of Co^{2+} in water pollutants, such as nanofiltration, adsorption, and ion exchange, in which the adsorption process is the best choice because it is cheap and suitable to adapt with a vast range of working conditions to remove Co^{2+} ion from aqueous solutions [4–10]. In order to improve the adsorption efficiency, some advanced nanomaterials have been applied for enhancing the specific surface area of the adsorbent which favors adsorption using carbon nanotubes (CNTs) [11–13], activated carbon [14, 15], graphite [16], graphene oxide (GO) [17], or reduced graphene oxide [18]. These nanomaterials have many functional groups on the surface such as –COOH, –OH, and C=O which can be used as an electron-trapping site to attract metal ions or organic materials [11–14, 17]. Recently, GO is widely applied as an adsorbent directed to adsorb heavy metal ions from water because GO has a large surface area (which can be up to 2630 $m^2\cdot g^{-1}$) and high water solubility [19–22]. In addition, GO has abundant oxygen-based groups on its surface such as hydroxyl, carboxylic, carbonyl, and epoxide groups, making GO a material of great interest in adsorption-based technologies of water treatment. GO adsorbents with excellent maximum adsorption capacity (q_{max}) were reported, such as $q_{max} = 198\ mg\cdot g^{-1}$ for adsorption of Cr(VI) ion [23] and the $q_{max} = 46.6\ mg\cdot g^{-1}$ for adsorption of Cu(II) ion [24]. However, GO is a nano/micromaterial and it has very low density; therefore, it is difficult to remove GO out of the water after adsorption

processes. The hybrids of graphene with magnetic nanomaterials such as Fe_3O_4 nanoparticles have been used to solve the above problem. Fe_3O_4 is usually used for water purification due to its safety; in addition, the Fe_3O_4 is also used to generate magnetic properties for the adsorbent, which makes it easy to be collected after treatment by using an external magnet bar. Yao et al. [25] reported Fe_3O_4@graphene in dye removal with q_{max} of 45.27 mg·g^{-1} to methylene blue (MB) and 33.66 mg·g^{-1} to Congo red [25]. Uheida et al. [26] has used Fe_3O_4 and ɣ-Fe_2O_3 nanoparticles for the removal of Co^{2+} ion. To improve the bonding of Fe_3O_4 nanoparticles with the GO sheets, a natural polymer or synthetic polymer can be used. In fact, polyvinyl alcohol (PVA) is widely used in the adsorption process because of its nontoxicity, low cost, and chemical stability and having many hydroxyl (-OH) groups [27, 28]. Wang et al. [28] have fabricated the GO-PVA composites and showed that GO-PVA can adsorb MB with a q_{max} of 571.4 mg·g^{-1}. We have reported the use of GO/chitosan/Fe_3O_4 nanocomposite as a recoverable and recyclable adsorbent for Cr(IV) ion adsorption with easy removal of the GO/chitosan/Fe_3O_4 composite adsorbent out of the solution by using a magnetic bar and especially high adsorption capacity (q_{max} = 200 mg·g^{-1}) for Cr(IV) ion [29]. In this study, we extend the above approach with chitosan being replaced by PVA for synthesis of the GO/PVA/Fe_3O_4 composite, which was directed to adsorb of Co^{2+} ion.

2. Experimental

2.1. Materials and Reagents. Concentrated sulfuric acid (H_2SO_4 98 wt.%), ammonium iron (II) sulfate hexahydrate ($(NH_4)_2Fe(SO_4)_2.6H_2O$, 99 wt.%), ethanol (C_2H_5OH, 96 v/v.%), and hydrochloric acid (HCl) were purchased from Duc Giang Chemical Co., Ltd. (Vietnam). Potassium sulfate (K_2SO_4, 99 wt.%), iron(III) chloride hexahydrate ($FeCl_3.6H_2O$, 99 wt.%), sodium hydroxide (NaOH, 99 wt.%), and acetic acid (CH_3COOH, 99 wt.%) were purchased from Xilong (China). Polyvinyl alcohol (PVA) ($M_w \approx 47\ 000$, 87–90% hydrolyzed), ammonium thiocyanate (NH_4SCN, ≥wt.%), and acetone were purchased from Sigma-Aldrich. Aqueous ammonia is an analytical reagent and used without further purification. GO was purchased from Graphitene Ltd., and $CoCl_2.6H_2O$ (≥99 wt.%) was purchased from Merck.

2.2. Preparation of Fe_3O_4 Nanoparticles. Fe_3O_4 nanoparticles were prepared by the coprecipitation method. First, 0.951 g of $FeCl_3.6H_2O$ and 0.69 g of $(NH_4)_2Fe(SO_4)_2.6H_2O$ were dissolved in 50 ml of distilled water. Then, 10 wt.% ammonia solution is added drop by drop to adjust pH of the solution to 8-9. The black precipitate of Fe_3O_4 will be obtained.

2.3. Preparation of GO/PVA/Fe_3O_4 Nanocomposite. 0.1 g of GO was ultrasonicated in 30 ml of distilled water at ambient conditions to have a slurry solution. 0.2 g of PVA was dissolved in 30 ml of distilled water and stirred at 500 rpm at 90°C. When all PVA is dissolved completely and GO is dispersed well, they are mixed with a mixture of Fe_3O_4 colloid, stirred for 10 minutes and filtered, washed many times with distilled water, and finally dried in an oven at 40°C for 1 day.

2.4. Batch Adsorption Experiments for Co^{2+} Ion Removal. 0.0406 g of $CoCl_2.6H_2O$ was dissolved in 100 mL distilled water to obtain the stock solution of Co^{2+} ion (100 mg·L^{-1}). The stock solution was diluted to the desired solution. 0.01 g of GO/PVA/Fe_3O_4 nanocomposite as an adsorbent was added into 20 mL of the solution containing Co^{2+} ion; then, the mixtures were agitated at 30°C and pH 7 for 100 min. The residue Co^{2+} ion concentration in the solution was analysed by the spectrophotometric method (described in Section 3.5). The adsorption capacity, q (mg·g^{-1}), and the percentage removal (H, %) were calculated by the following equations:

$$q = \frac{(C_0 - C)\cdot V}{m}\left(mg\cdot g^{-1}\right),$$
$$H = \frac{(C_0 - C_e)}{C_0}\cdot 100\%\ (\%), \quad (1)$$

where C_0 and C_e are the initial and equilibrium concentrations of Co^{2+} solution (mg·L^{-1}), respectively; C is the Co^{2+} ion concentration at time t; V is the volume of the sample solution used for the experiment (mL); and m is the weight of the adsorbent (g). The adsorption of Co^{2+} ion onto GO/PVA/Fe_3O_4 was studied as a function of contact time, mass of adsorbent influent, pH of the solution, and temperature.

The used GO/PVA@Fe_3O_4 adsorbent was recovered by immersing it into 0.1 N NaOH solution for 1 day, and then, it was rinsed with distilled water and dried at 40°C in an oven for 12 h to obtain the regenerated GO/PVA@Fe_3O_4 adsorbent, which was reused to adsorb Co^{2+} ion.

2.5. Determination of Co^{2+} Ion Concentration. The Co^{2+} ion concentration after adsorption process is determined by the spectrophotometric method with the aid of many complexing reagents, which had been developed recently to monitor Co^{2+} concentration, with fast response, high sensitivity, and easy preparation compared to other methods. The common complexing reagents used include ninhydrin (optimum pH is 8.2; the complex is stable in 30 min) [30], 2-benzoylpyridine-4-phenyl-3-thiosemicarbazone [31], 2-pyridine carboxaldehyde isonicotinyl hydrazone (pH 9; the apparent molar adsorptivity is 7.1.10^4 L·mol^{-1}·cm^{-1}) [32], dehydroacetic acid oxime (pH 5.8) [33], and 5-[3-(1,2,4-triazolyl-azo]-2,4-dihydroxybenzaldehyde [34]. In our work, we used NH_4SCN as a ligand in acetone solution and we have discovered that it can be stable up to more than 7 days. A typical procedure is followed: 1 ml of 18% HCl solution is added into 10 ml of residue solution at RT. Then, 0.5 ml of NH_4SCN saturated solution is added into the above mixture and the solution is mixed well. After that, 20 ml of concentrated acetone is added into this mixture and the solution will change from pink color to blue color in the following reaction:

$$CoCl_2 + 4NH_4SCN \longrightarrow \underset{\text{(pink color)}}{(NH4)_2[Co(SCN)4]} + 2NH_4Cl \quad \underset{\text{(blue color)}}{} \tag{2}$$

The absorbance of the mixture is then measured with an Agilent 8453 UV-Vis spectrophotometer, and the calibration curve is obtained (Figure S1). Each sample was measured in duplicate.

2.6. Characterizations. XRD patterns of GO and GO/PVA/Fe_3O_4 were obtained on D8 Advance, Brucker ASX, operated at a CuK_α wavelength of 1.542 $\dot{A}$ in the range of $2\theta = 5$ to 70° at the room temperature. UV-Vis spectra were measured with an Agilent 8453 UV-Vis spectrophotometer system. The fracture surfaces of GO and GO/PVA/Fe_3O_4 were observed using a Hitachi S4500 Scanning Electron Microscope (SEM). The infrared (IR) spectra were recorded on a Nicolet FT-IR Spectrometer model 205 with KBr pellets in the region from 500 cm^{-1} to 4000 cm^{-1}. Specific surface area and pore size distribution of the prepared GO/PVA/Fe_3O_4 sample were evaluated using low-temperature nitrogen adsorption isotherm by Brunauer-Emmett-Teller (BET) and Barrett-Joyner-Halenda (BJH) methods on the Tristar II plus System (Micromeritics, USA).

3. Results and Discussion

3.1. Characterization of the GO/PVA/Fe_3O_4 Nanocomposite. The XRD patterns of GO and GO/PVA/Fe_3O_4 (Figure 1(a)) show a diffraction peak at $2\theta = 10°$, which is assigned to the crystalline of GO (curve A) with (001) reflection indicating that the oxygen functionality existence increases the distance between graphene layers. Using Bragg's Law and Scherrer equation for this sharp peak, it is revealed that the interlayer space is about 0.885 nm and the number of layers in GO is 5. In case of GO/PVA/Fe_3O_4 (curve b), this peak disappears due to a very low content of GO in the sample; however, the characteristic peaks of Fe_3O_4 clearly appeared at $2\theta = 30°$, 35°, 57°, and 63° corresponding to the reflection of (220), (311), (511), and (440), respectively.

The FT-IR spectrum of GO/PVA/Fe_3O_4 (Figure 1(b), curve C) shows the band at 3221 cm^{-1}, which denotes to the –OH stretching of physisorbed water. The band at 2902 cm^{-1} attributed to the C-H stretching vibration, and the characteristic peaks ascribed to C-OH groups (1413 cm^{-1} and 1078 cm^{-1}) in PVA were found in both the FT-IR spectrum of PVA and GO/PVA/Fe_3O_4 (Figure 1(b), curve B and curve C, respectively) confirming the presence of PVA in the GO/PVA/Fe_3O_4 samples. A peak at 542 cm^{-1} is attributed to the Fe-O group of Fe_3O_4 in GO/PVA/Fe_3O_4 samples (curve C), indicating that Fe_3O_4 is linked successfully to the GO and PVA. SEM images of GO (Figures 1(c) and 1(e)) show that the GO materials are arranged in sheets. SEM images of the GO/PVA/Fe_3O_4 adsorbent (Figures 1(d) and 1(f)) show an appearance of spherical particles with a size of about 15–20 nm, deposited on the GO sheets, nearly covering all the surface of GO sheets, making it difficult to see the GO sheets. It can be seen the Fe_3O_4 nanoparticles were well distributed on the GO sheets (Figure 1(f)); these Fe_3O_4 nanoparticles contribute to making the magnetic property recover the GO/PVA/Fe_3O_4 adsorbent from the solution after the adsorption process by using an external magnet. The hysteresis loop of the nitrogen adsorption-desorption isotherm of the GO/PVA/Fe_3O_4 nanocomposite (Figure 1(g)) exhibits type IVa hysteresis loops by IUPAC, which is specific to mesoporous materials with a pore width range from 4 to 50 nm [35]. The BJH pore size distribution of GO/PVA/Fe_3O_4 sample (Figure 1(h)) shows the main pore diameters to be less than 7 nm, which is in agreement with the shape of the hysteresis loop above (Figure 1(g)). The BET specific surface area and BJH average pore width of the synthesized GO/PVA/Fe_3O_4 sample is summarized in Table 1.

3.2. Optimization Conditions for Co^{2+} Ion Adsorption onto GO/PVA/Fe_3O_4 Nanocomposite. Figure 2(a) shows that Co^{2+} ion adsorption capacity increased rapidly when contact time was from 3 to 100 minutes, with about 60% of the Co^{2+} removed, and thereafter, the adsorption capacity has a constant trend. The rapid uptake within 100 min was due to the large surface area, the presence of various oxygen functional groups of GO, and PVA that creates an electrostatic interaction with Co^{2+} ion. After that, the adsorption sites of the adsorbent were filled with Co^{2+} ions so the rate of adsorption becomes constant. The contact time here longer than that in other reported materials [36] can be attributed to higher of Co^{2+} initial concentration and lower used adsorbent dose (100 $mg{\cdot}L^{-1}$, $m = 0.01$ g) as well. The influence of adsorbent dosage was evaluated by changing the mass of GO/PVA/Fe_3O_4 adsorbent from 0.0123 g to 0.034 g for treatment of 20 mL of Co^{2+} solution, and the obtained results show that with the increasing mass of the adsorbent, the adsorption capacity decreases and the optimal amount of absorbent is 0.0123 g with an adsorption capacity q_e is 17.63 $mg\,g^{-1}$ (Figure 2(b)). Figure 2(c) reveals that the q_e increased with the increase in temperature, which suggested that the adsorption of Co^{2+} ion onto the GO/PVA/Fe_3O_4 adsorbent may be favored by high temperature and therefore the optimal temperature for this process was selected at 50 C.

The influence of pH on the adsorption process was evaluated with pH change from pH 2 to pH 7 because at higher pH (pH > 7), Co^{2+} ion can be agglomerated as a $Co(OH)_2$ precipitate [37, 38]. As shown in Figure 2(d), Co^{2+} ion removal was 61.7% with a q_e of 121 $mg{\cdot}g^{-1}$ at pH 2 (curve A) and the removal was about 64.0% with a q_e of 127.3 $mg{\cdot}g^{-1}$ at pH 5.2 (curve B), and the UV-Vis spectra at equilibrium time are shown in Figure S2. The obtained results can explain that the high concentration of H^+ ion (at low pH value) led to the competition between positive charge ions to attach with negative charge oxygen functional groups on GO and PVA. Meanwhile, at higher pH, the concentration of H^+ ions decreases so there is less competition, and the result is the adsorption increase. Therefore, the optimal pH for adsorption Co^{2+} ion onto GO/PVA/Fe_3O_4 was pH 5.2. Effect of K^+ ion as an interference to the adsorption of Co^{2+} onto GO/PVA/Fe_3O_4 was also tested (Table 2). Results show that the presence of K^+ ion did not

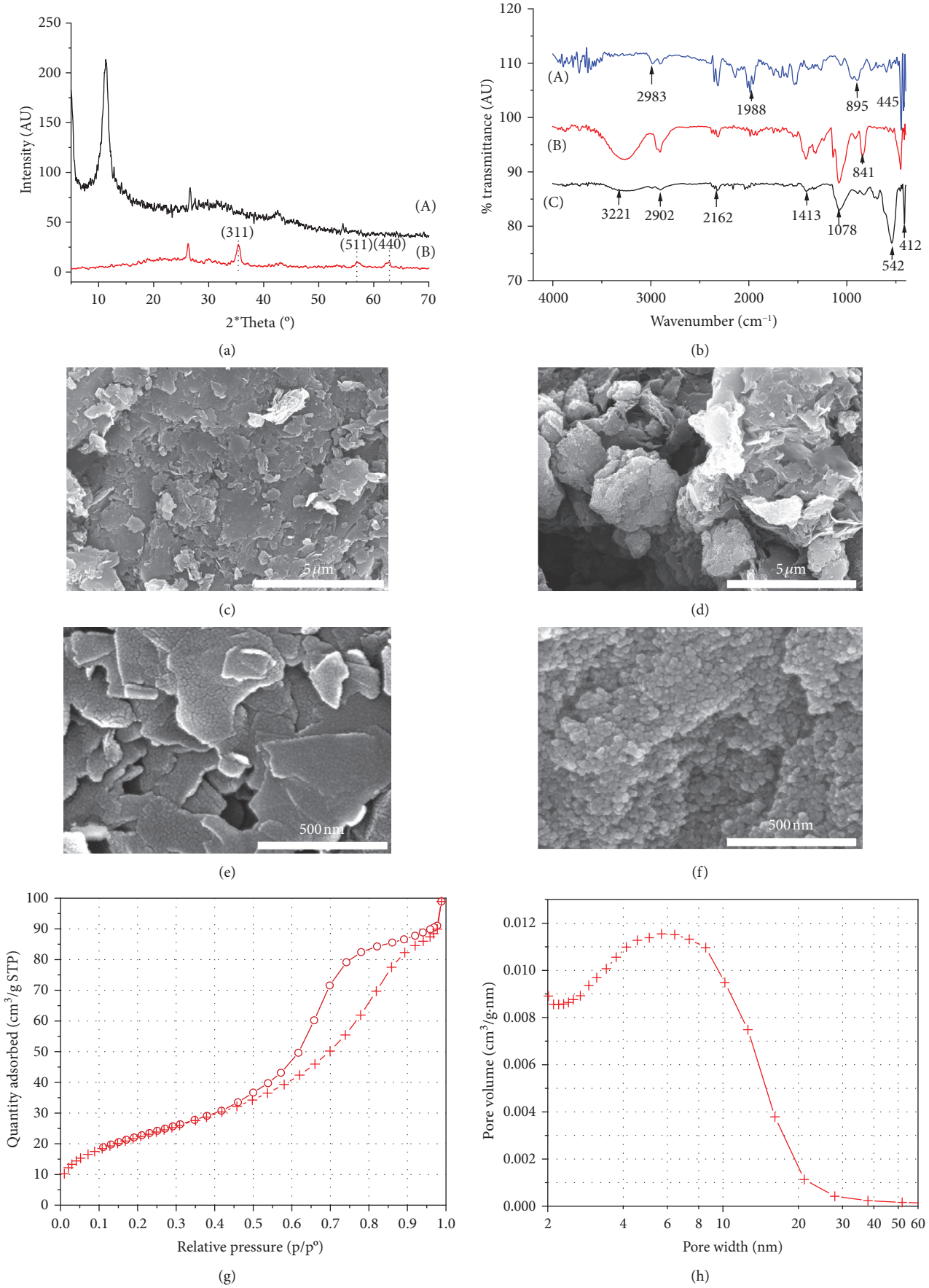

Figure 1: (a) XRD patterns of GO (A) and GO/PVA/Fe_3O_4 (B) sample; (b) FT-IR of GO (A), PVA (B), and GO/PVA/Fe_3O_4 (C); (c–f) SEM images with different magnifications of (c, e) GO and (d, f) GO/PVA/Fe_3O_4, respectively; nitrogen (N_2) adsorption-desorption isotherm (g) and BJH pore size distribution (h) of the as-synthesized GO/PVA/Fe_3O_4 sample.

Table 1: BET surface area analysis of as-synthesized GO/PVA/Fe_3O_4 sample.

Surface area ($m^2 \cdot g^{-1}$)			BJH pore volume ($cm^3 \cdot g^{-1}$)	BJH average pore width (nm)
Langmuir surface area	BET surface area	BJH pore area		
122.328 ± 3.367	82.071 ± 0.163	97.218	0.137 ÷ 0.144	5.931 ÷ 6.725

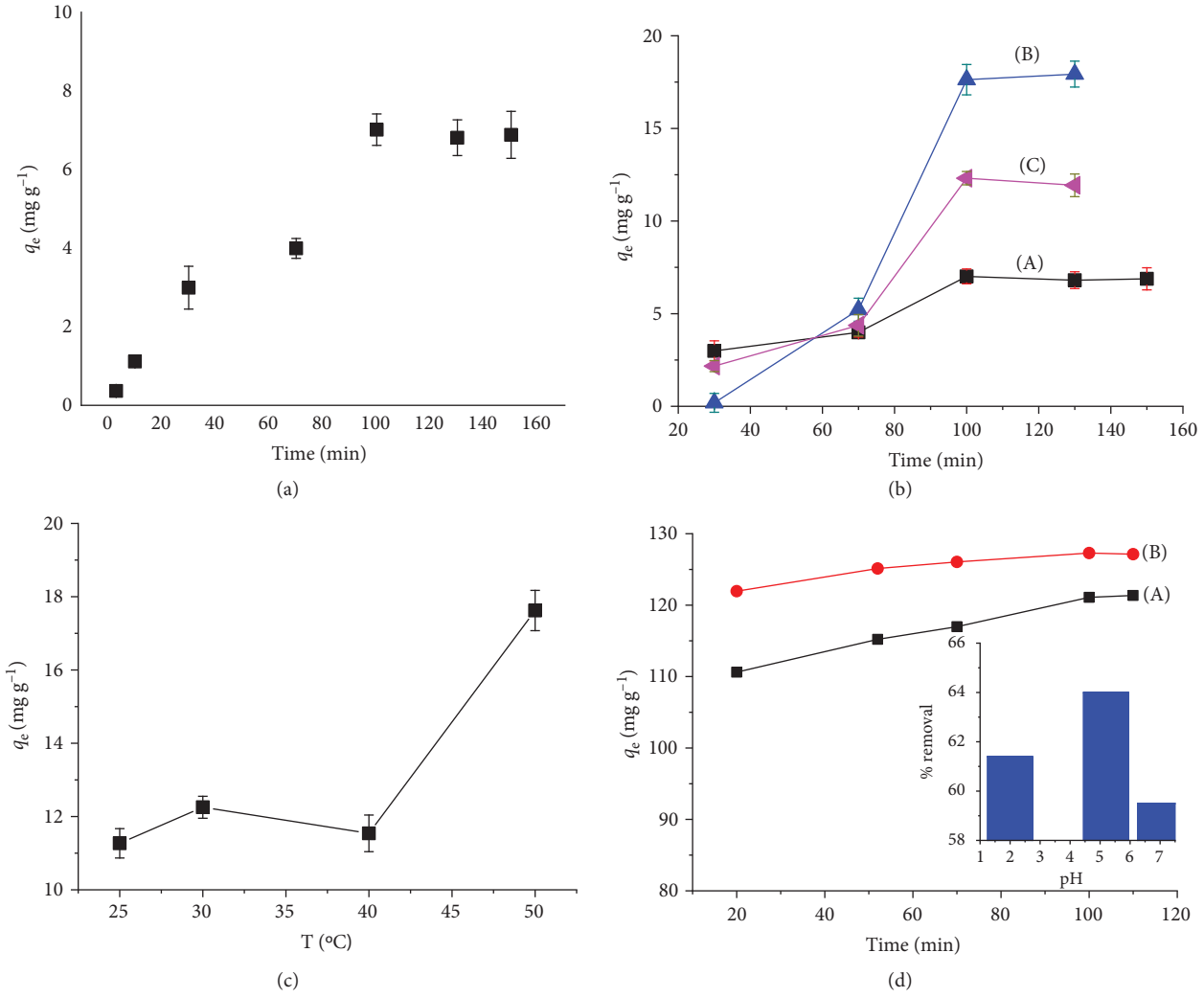

Figure 2: Optimization conditions for adsorption Co^{2+} ion onto GO/PVA/Fe_3O_4 nanocomposite: (a) effect of contact time, (b) effect of the adsorbent dosage: (A) 0.03 g; (B) 0.02 g; (C) 0.01 g, respectively, (c) effect of temperature, and (d) effect of pH: (A) pH 2 and (B) pH 5.2 (inserted image: % removal of samples vs. pH).

Table 2: The effect of K^+ as an interfering ion to the adsorption of Co^{2+} ion onto GO/PVA/Fe_3O_4 nanocomposite(*).

Interfering ion	Fold ratio	Adsorption efficiency (%)
K^+	10	63.7
K^+	20	61.9
K^+	50	62.3
K^+	80	63.0

(*)Experimental conditions: $C_o = 100\ mg \cdot g^{-1}$, pH = 5.2, $T = 25$ C, and $m_{adsorbent} = 0.01$ g.

interfere with the adsorption efficiency of Co^{2+} ion, even when the concentration of interfering K^+ ion was 10–80 times higher than the Co^{2+} ion concentration, which is completely consistent with the previous report [39].

3.3. The Kinetics of Co^{2+} Ion Adsorption onto GO/PVA/Fe_3O_4 Nanoadsorbent. In this work, two kinetic models including the pseudo-first-order and the pseudo-second-order

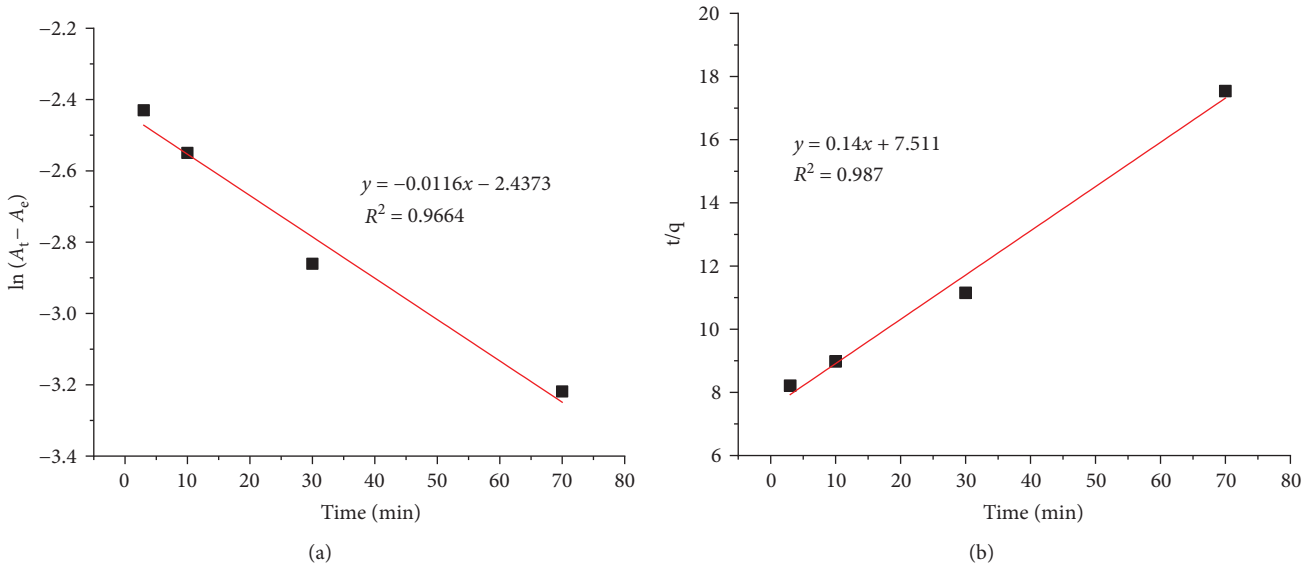

FIGURE 3: (a) $\ln(A_t - A_e)$ vs. t plot and (b) t/q vs. t plot to calculate the rate constant. Experimental conditions: $m_{adsorbent} = 0.034$ g, $T = 30^{\circ}$C, pH = 7, and $C_o = 20$ mg·L^{-1}.

kinetic models were analysed, which can be represented as follows:

$$\ln(q_e - q_t) = \ln q_e - k_1 t,$$
$$\frac{t}{q_t} = \frac{1}{k_2 \cdot q_e^2} + \frac{t}{q_e}, \tag{3}$$

where q_e is the adsorption capacity at equilibrium, q_t is the adsorption capacity at time t (min), and k_1 is the pseudo-first-order rate constant of adsorption (min^{-1}), and k_2 is the pseudo-second-order rate constant of adsorption (g·mg^{-1}·min^{-1}). As proved in the previous study [40], equation (2) can be written as follows:

$$\ln \frac{C_t}{C_0} = \ln\left(\frac{A_t - A_e}{A_t - A_0}\right) = -k_1 \cdot t, \tag{4}$$

where C_0 and C_t are the initial concentration and concentration of Co^{2+} ion in solution, respectively, A_o and A_e are the initial and equilibrium absorbance; k_1 was calculated from the slope of the plot of ln $(A_t - A_e)$ vs. t (Figure 3(a)); and k_2 was calculated from the slope of the plot of t/q_t vs. t. (Figure 3(b)). Based on comparison of the correlation coefficient (R^2) of two plots, it can be seen that the adsorption of Co^{2+} ion onto the GO/PVA/Fe_3O_4 adsorbent was fitted to the pseudo-second-order kinetic model than the pseudo-first-order kinetic model. The rate constant k_2 was fitted at 0.0026 g·mg^{-1}·min^{-1}.

3.4. Investigation of the Thermodynamic Parameters of the Adsorption Process. The thermodynamic parameters of the adsorption process such as enthalpy change (ΔH^0), entropy change (ΔS^0), and Gibbs free enthalpy change (ΔG^0) of reaction are calculated following the second law of thermodynamics, which have been described by the following equations:

$$\Delta G^0 = \Delta H^0 - T \cdot \Delta S^0 = -R \cdot T \cdot \ln K_c,$$
$$K_C = \frac{q_e}{C_e}, \tag{5}$$
$$\ln K_c = \frac{-\Delta H^0}{R} \cdot \frac{1}{T} + \frac{\Delta S^0}{R},$$

where R is the gas constant ($R = 8.314$ J·mol^{-1}·K^{-1}), K_c is the equilibrium constant of chemical reaction, and T is the absolute temperature (K). ΔH^0 and ΔS^0 can be calculated from the slope and the intercept on the plot of $\ln K_C$ vs. $1/T$ following equation (4) and the obtained results are given in Table 3. The negative value of ΔG^0 indicates that the process is spontaneous for all evaluated temperatures. The positive value of ΔH^0 confirms that the adsorption is endothermic and favors at high temperature. The positive value of ΔS^0shows the increase in the randomness of the adsorption on GO/PVA/Fe_3O_4 for Co^{2+} ion.

3.5. Adsorption Isotherm. The Langmuir model (equation (5)) assumes a monolayer adsorption onto the homogeneous surface, and there is no transmigration of adsorbate on the surface plane. Meanwhile, the Freundlich model assumes a multilayer adsorption onto the heterogeneous surface (equation (5)).

$$\frac{C_e}{q_e} = \frac{1}{(K_L \cdot q_{max})} + \frac{1}{q_{max}} \cdot C_e,$$
$$\lg q_e = \lg K_F + \frac{1}{n} \cdot \lg C_e, \tag{6}$$

Table 3: Thermodynamic parameters of the adsorption Co^{2+} ion on GO/PVA/Fe_3O_4.

ΔG^0 (kJ·mol^{-1})				ΔH^0 (kJ·mol^{-1})	ΔS^0 (J·mol^{-1}·K^{-1})
298 K	303 K	313 K	323 K	22.04	106.47
−9.8	−10.07	−10.06	−12.38	—	—

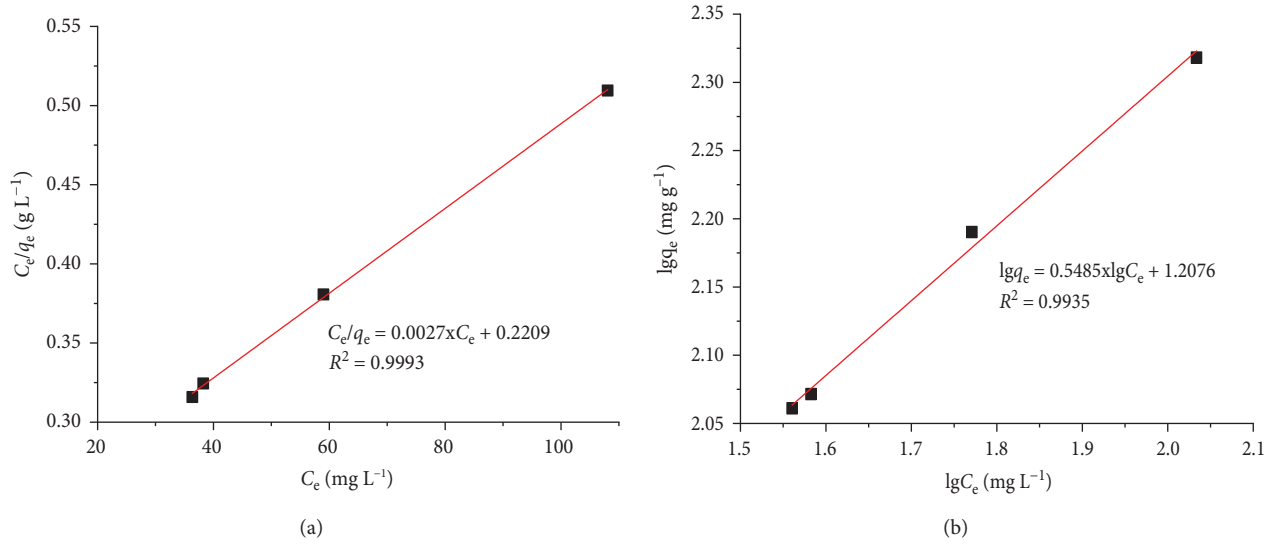

Figure 4: Adsorption isotherm following (a) Langmuir and (b) Freundlich models for Co^{2+} ion adsorption onto the GO/PVA/Fe_3O_4, nanocomposite. Experimental conditions: pH = 5.2, C_0 = 100–250 mg·L^{-1}, T = 303 K, and $m_{adsorbent}$ = 0.01 g.

Table 4: The Langmuir and Freundlich isotherm parameters.

Langmuir isotherm			Freundlich isotherm		
q_{max} (mg·g^{-1})	K_L	R^2	K_F	N	R^2
370.37	0.0122	0.9993	15.8767	0.5485	0.9935

where q_{max} (mg·g^{-1}) is the maximum adsorption capacity of Co^{2+} ion onto the GO/PVA/Fe_3O_4 adsorbent; K_L, K_F are the Langmuir constant and Freundlich constant, respectively; and n is a constant. Experimental results following the Langmuir and Freundlich adsorption isotherm are shown in Figure 4, and the fitting of the Langmuir and Freundlich constants is given in Table 4. It can be seen that, with the higher correlation coefficient, the Langmuir model fitted well for the adsorption of Co^{2+} ion onto GO/PVA/Fe_3O_4 (Table 4). The maximum monolayer adsorption capacity q_{max} is 370.37 mg·g^{-1} and K_L is 0.0122. Compared to the other adsorbents in the literature for Co^{2+} ion removal (Table 5), the obtained result in our work is so high and impressive, which can be attributed to a very large surface area of GO, facilitating the adsorption process.

3.6. Recordation and Regeneration Studies. SEM images of GO/PVA/Fe_3O_4 adsorbent before (Figure 5(a)) and after Co^{2+} adsorption process (Figure 5(b)) are not significantly different excepting several clusters of particles appearing on the surface of adsorbent after the adsorption process, and the surface of the GO/PVA/Fe_3O_4 adsorbent after adsorption process is less porous than that before. These observations

Table 5: Comparison of various adsorbents for Co^{2+} ion removal.

Adsorbent materials	q_{max} (mg·g^{-1})	Ref.
Palygorskite	8.88	[41]
Lignocellulose/montmorillonite	93.43	[42]
Fe_3O_4/bentonite	18.76	[43]
Hydroxyapatite	22.50	[44]
GO/PVA/Fe_3O_4	370.37	This work

can be attributed to the presence of adsorbed Co^{2+} ion onto the GO/PVA/Fe_3O_4 surface, which was confirmed by the EDS analyses. It can be seen that there was no cobalt element (0 wt.%) on the EDS spectrum of GO/PVA/Fe_3O_4 before adsorption (Figure 5(c)); meanwhile, with the sample after Co^{2+} ion adsorption, the cobalt element reached 4 wt.% (Figure 5(d)), in which Co^{2+} ions were adsorbed onto the GO/PVA/Fe_3O_4 adsorbent.

As shown in FIgure S3, the regenerated GO/PVA/Fe_3O_4 adsorbent can adsorb Co^{2+} ion with only a small decrease in adsorption capacity between the 1st cycle and the 5th cycle. The remaining adsorption efficiency of the 5th cycle was about 86% of the 1st cycle (Figure S3), which implies that the GO/PVA/Fe_3O_4 material has a good stability and a high

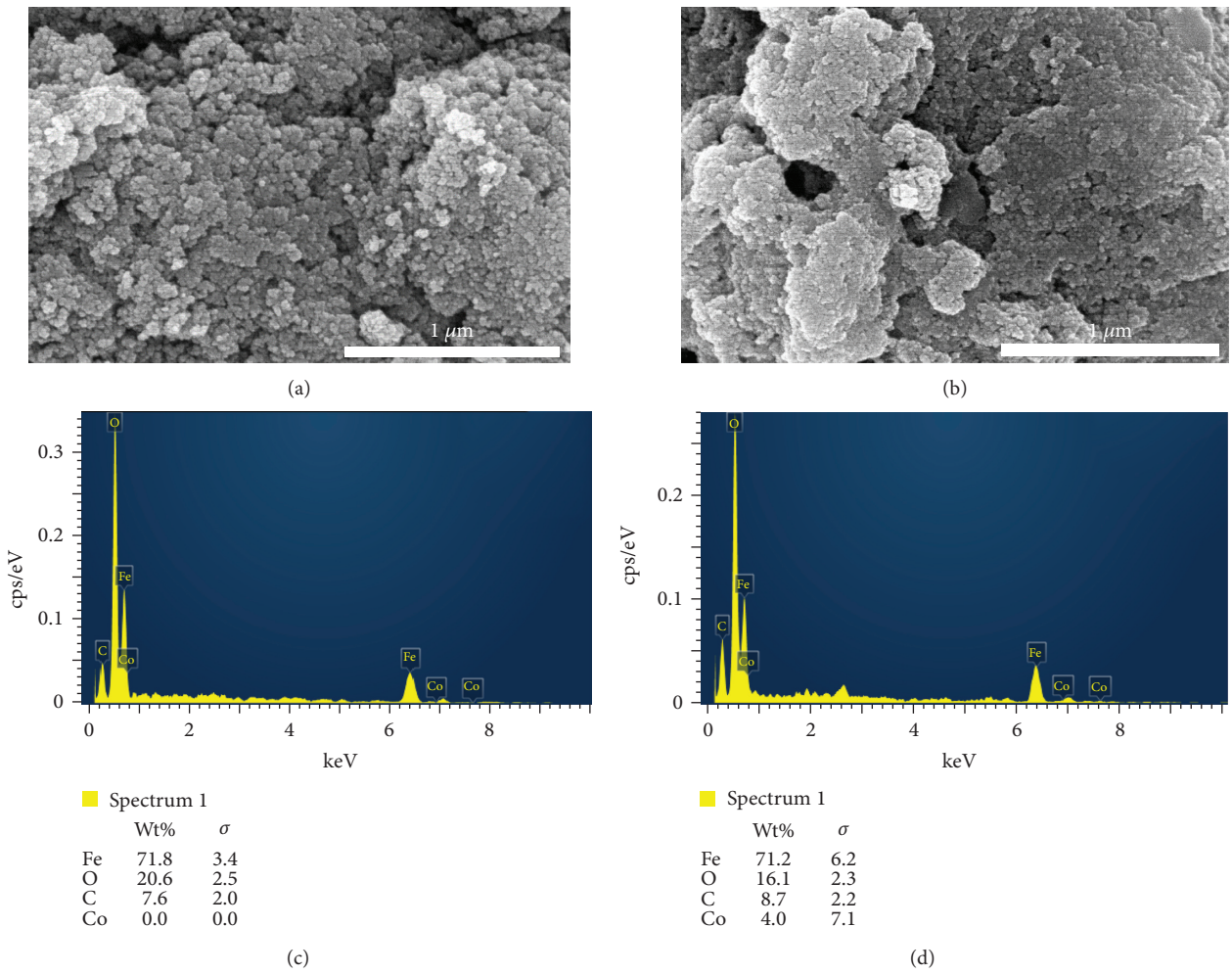

Figure 5: (a, b) SEM and (c, d) EDS spectra of the adsorbent before (a, c) and after (b, d) Co^{2+} ion adsorption process.

degree of regeneration to use as an excellent adsorbent for removal of Co^{2+} ion in aqueous solution.

4. Conclusion

As described in this study, GO/PVA/Fe_3O_4 nanocomposite as an effective adsorbent has been simply synthesized via a coprecipitation technique and it was directed to capture Co^{2+} ions from an aqueous solution via an adsorption process. The adsorption process of Co^{2+} ion onto the GO/PVA/Fe_3O_4 adsorbent was evaluated by studying the effects of adsorbent dose, the solution pH, and temperature. At optimized adsorption conditions, this process followed the pseudo-second-order kinetic model and the adsorption isotherm was fitted to the Langmuir model with the maximum adsorption capacity to Co^{2+} ion estimated at 370.37 $mg{\cdot}g^{-1}$. The GO/PVA/Fe_3O_4 adsorbent can be regenerated for at least 5 cycles with the remaining adsorption efficiency after the 5th cycle being 86% compared to the first cycle. These findings indicate that the GO/PVA/Fe_3O_4 nanocomposite can be considered as a good candidate for the removal of Co^{2+} ion from aqueous solutions.

Data Availability

The data used to support the findings of this study are included within the article.

Conflicts of Interest

The authors declare that they have no conflicts of interest.

Acknowledgments

This work was supported by the Ministry of Education Project, under code number B2020-BKA-15.

Supplementary Materials

Figure S1(a) UV-Vis spectra of various concentrations of Co^{2+} solution and (b) the calibration curve for Co^{2+} concentration measurement. Figure S2The UV-Vis spectra of samples at different pH values vs. equilibrium time: (i) pH 2 and (ii) pH 5.2. Experimental conditions: adsorbent dose 0.01 g, initial concentration of Co^{2+} ion 100 $mg{\cdot}L^{-1}$, and temperature 25°C. Figure S3GO/PVA/Fe_3O_4 regeneration results. Conditions: adsorbent dose 0.01 g, initial

concentration of Co^{2+} ions 100 mg·L^{-1}, temperature 25°C, and pH = 5.2. (*Supplementary Materials*)

References

[1] F. Zheng, Z. Luo, C. Zheng et al., "Comparison of the neurotoxicity associated with cobalt nanoparticles and cobalt chloride in Wistar rats," *Toxicology and Applied Pharmacology*, vol. 369, pp. 90–99, 2019.

[2] M. Abbas, M. Adil, S. Ehtisham-ul-Haque et al., "Vibrio fischeri bioluminescence inhibition assay for ecotoxicity assessment: a review," *Science of The Total Environment*, vol. 626, pp. 1295–1309, 2018.

[3] M. Iqbal, "Vicia faba bioassay for environmental toxicity monitoring: a review," *Chemosphere*, vol. 144, pp. 785–802, 2016.

[4] A. E. Burakov, E. V. Galunin, I. V. Burakova et al., "Adsorption of heavy metals on conventional and nanostructured materials for wastewater treatment purposes: a review," *Ecotoxicology and Environmental Safety*, vol. 148, pp. 702–712, 2018.

[5] A. Awwad, M. Amer, and M. Al-aqarbeh, "TIO2-Kaolinite nanocomposite prepared from the Jordanian kaolin clay: adsorption and thermodynamics of Pb(II) and Cd(II) ions in aqueous solution," *Chemistry International*, vol. 6, pp. 168–178, 2020.

[6] A. Kanwal, H. N. Bhatti, M. Iqbal, and S. Noreen, "Basic dye adsorption onto clay/$MnFe_2O_4$ composite: a mechanistic study," *Water Environment Research*, vol. 89, no. 4, pp. 301–311, 2017.

[7] G. Sharma and M. Naushad, "Adsorptive removal of noxious cadmium ions from aqueous medium using activated carbon/zirconium oxide composite: isotherm and kinetic modelling," *Journal of Molecular Liquids*, vol. 310, 2020.

[8] M. Naushad, "Surfactant assisted nano-composite cation exchanger: development, characterization and applications for the removal of toxic Pb^{2+} from aqueous medium," *Chemical Engineering Journal*, vol. 235, pp. 100–108, 2014.

[9] M. Naushad, A. Mittal, M. Rathore, and V. Gupta, "Ion-exchange kinetic studies for Cd(II), Co(II), Cu(II), and Pb(II) metal ions over a composite cation exchanger," *Desalination and Water Treatment*, vol. 54, no. 10, pp. 2883–2890, 2015.

[10] S. M. Shaheen, J. Rinklebe, T. Frohne, J. R. White, and R. D. DeLaune, "Redox effects on release kinetics of arsenic, cadmium, cobalt, and vanadium in Wax Lake Deltaic freshwater marsh soils," *Chemosphere*, vol. 150, pp. 740–748, 2016.

[11] Y.-H. Li, S. Wang, J. Wei et al., "Lead adsorption on carbon nanotubes," *Chemical Physics Letters*, vol. 357, no. 3-4, pp. 263–266, 2002.

[12] J. Zhao, A. Buldum, J. Han, and J. P. Lu, "Gas molecule adsorption in carbon nanotubes and nanotube bundles," *Nanotechnology*, vol. 13, no. 2, pp. 195–200, 2002.

[13] C. Chen and X. Wang, "Adsorption of Ni(II) from aqueous solution using oxidized multiwall carbon nanotubes," *Industrial & Engineering Chemistry Research*, vol. 45, no. 26, pp. 9144–9149, 2006.

[14] A. Namane, A. Mekarzia, K. Benrachedi, N. Belhanechebensemra, and A. Hellal, "Determination of the adsorption capacity of activated carbon made from coffee grounds by chemical activation with ZnCl and HPO," *Journal of Hazardous Materials*, vol. 119, no. 1-3, pp. 189–194, 2005.

[15] Ihsanullah, F. A. Al-Khaldi, B. Abusharkh et al., "Adsorptive removal of cadmium(II) ions from liquid phase using acid modified carbon-based adsorbents," *Journal of Molecular Liquids*, vol. 204, pp. 255–263, 2015.

[16] D. laoui, L. Österlund, and B. Kasemo, "Water adsorption on graphite (0001)," *Vacuum*, vol. 46, no. 8-10, pp. 1109–1112, 1995.

[17] S. Thangavel and G. Venugopal, "Understanding the adsorption property of graphene-oxide with different degrees of oxidation levels," *Powder Technology*, vol. 257, pp. 141–148, 2014.

[18] K. Gupta and O. P. Khatri, "Reduced graphene oxide as an effective adsorbent for removal of malachite green dye: plausible adsorption pathways," *Journal of Colloid and Interface Science*, vol. 501, pp. 11–21, 2017.

[19] S. Thangavel, S. Thangavel, N. Raghavan, K. Krishnamoorthy, and G. Venugopal, "Visible-light driven photocatalytic degradation of methylene-violet by rGO/Fe_3O_4/ZnO ternary nanohybrid structures," *Journal of Alloys and Compounds*, vol. 665, pp. 107–112, 2016.

[20] V. Pandiyarasan, J. Archana, A. Pavithra et al., "Hydrothermal growth of reduced graphene oxide on cotton fabric for enhanced ultraviolet protection applications," *Materials Letters*, vol. 188, pp. 123–126, 2017.

[21] A. Fakhri, "Adsorption characteristics of graphene oxide as a solid adsorbent for aniline removal from aqueous solutions: kinetics, thermodynamics and mechanism studies," *Journal of Saudi Chemical Society*, vol. 21, no. Supplement 1, pp. S52–S57, 2017.

[22] H.-L. Ma, Y. Zhang, Q.-H. Hu, D. Yan, Z.-Z. Yu, and M. Zhai, "Chemical reduction and removal of Cr(VI) from acidic aqueous solution by ethylenediamine-reduced graphene oxide," *Journal of Materials Chemistry*, vol. 22, no. 13, pp. 5914–5916, 2012.

[23] K. Zhang, H. Li, X. Xu, and H. Yu, "Synthesis of reduced graphene oxide/NiO nanocomposites for the removal of Cr(VI) from aqueous water by adsorption," *Microporous and Mesoporous Materials*, vol. 255, pp. 7–14, 2018.

[24] S.-T. Yang, Y. Chang, H. Wang et al., "Folding/aggregation of graphene oxide and its application in Cu^{2+} removal," *Journal of Colloid and Interface Science*, vol. 351, no. 1, pp. 122–127, 2010.

[25] Y. Yao, S. Miao, S. Liu, L. P. Ma, H. Sun, and S. Wang, "Synthesis, characterization, and adsorption properties of magnetic Fe_3O_4@graphene nanocomposite," *Chemical Engineering Journal*, vol. 184, pp. 326–332, 2012.

[26] A. Uheida, G. Salazar-Alvarez, E. Björkman, Z. Yu, and M. Muhammed, "Fe_3O_4 and γ-Fe_2O_3 nanoparticles for the adsorption of Co^{2+} from aqueous solution," *Journal of Colloid and Interface Science*, vol. 298, no. 2, pp. 501–507, 2006.

[27] Y. Li, P. Wang, C. Liu et al., "High strength polyvinyl alcohol/graphene oxide composite hydrogel," *Gaofenzi Cailiao Kexue Yu Gongcheng/Polymeric Materials Science and Engineering*, vol. 31, pp. 161–166, 2015.

[28] N. Wang, P. R. Chang, P. Zheng, and X. Ma, "Graphene-poly(vinyl alcohol) composites: fabrication, adsorption and electrochemical properties," *Applied Surface Science*, vol. 314, pp. 815–821, 2014.

[29] H. V. Tran, T. L. Tran, T. D. Le, T. D. Le, H. M. T. Nguyen, and L. T. Dang, "Graphene oxide enhanced adsorption capacity of chitosan/magnetite nanocomposite for Cr(VI) removal from aqueous solution," *Materials Research Express*, vol. 6, no. 2, 2018.

[30] K. Mahmood, F. H. Wattoo, M. H. S. Wattoo et al., "Spectrophotometric estimation of cobalt with ninhydrin," *Saudi Journal of Biological Sciences*, vol. 19, no. 2, pp. 247–250, 2012.

[31] H. Bingol and T. Atalay, "Study of kinetics of complexation reaction of Co^{2+} with 2-benzoylpyridine-4-phenyl-3-thiosemicarba zone and kinetic-spectrophotometric determination of cobalt," *Acta Physico-Chimica Sinica*, vol. 22, no. 12, pp. 1484–1488, 2006.

[32] S. Guzar and Q. Jin, "Simple, selective, and sensitive spectrophotometric method for determination of trace amounts of nickel(II), copper(II), cobalt(II), and iron(III) with a novel reagent 2-pyridine carboxaldehyde isonicotinyl hydrazone," *Chemical Research in Chinese Universities*, vol. 24, no. 2, pp. 143–147, 2008.

[33] J. Iqbal, F. Wattoo, S. Tirmizi, D. M. H. S. Wattoo, N. Ishrat, and A. Memon, "Dehydroacetic acid oxime as a new ligand for spectrophotometeric determination of cobalt," *Journal-Chemical Society of Pakistan*, vol. 29, no. 2, pp. 136–139, 2007.

[34] A. Khedr, M. Gaber, R. Issa, and H. Erten, "Synthesis and spectral studies of 5-[3-(1,2,4-triazolyl-azo]-2,4-dihydroxybenzaldehyde (TA) and its Schiff bases with 1,3-diaminopropane (TAAP) and 1,6-diaminohexane (TAAH). Their analytical application for spectrophotometric microdetermination of cobalt(II). Application in some radiochemical studies," *Dyes and Pigments*, vol. 67, no. 2, pp. 117–126, 2005.

[35] F. Sotomayor, K. A. Cychosz, and M. Thommes, "Characterization of micro/mesoporous materials by physisorption: concepts and case studies," *Accounts of Materials & Surface Research*, vol. 3, pp. 34–50, 2018.

[36] I. Bernabé, J. M. Gómez, E. Díez, P. Sáez, and A. Rodríguez, "Optimization and adsorption-based recovery of cobalt using activated disordered mesoporous carbons," *Advances in Materials Science and Engineering*, vol. 2019, no. 2, Article ID 3430176, 2019.

[37] K. A. Krishnan and T. S. Anirudhan, "Kinetic and equilibrium modelling of cobalt(II) adsorption onto bagasse pith based sulphurised activated carbon," *Chemical Engineering Journal*, vol. 137, no. 2, pp. 257–264, 2008.

[38] E. Demirbaş, "Adsorption of cobalt(II) ions from aqueous solution onto activated carbon prepared from hazelnut shells," *Adsorption Science & Technology*, vol. 21, no. 10, pp. 951–963, 2003.

[39] J. Fries and H. Getrost, *Organic Reagents for Trace Analysis*, E. Merck Darmstadt, Darmstadt, Hessen, Germany, 1977.

[40] L. T. Tran, H. V. Tran, T. D. Le, G. L. Bach, and L. D. Tran, "Studying Ni(II) adsorption of magnetite/graphene oxide/chitosan nanocomposite," *Advances in Polymer Technology*, vol. 2019, no. 3, Article ID 8124351, 2019.

[41] M. He, Y. Zhu, Y. Yang, B. Han, and Y. Zhang, "Adsorption of cobalt(II) ions from aqueous solutions by palygorskite," *Applied Clay Science*, vol. 54, no. 3-4, pp. 292–296, 2011.

[42] X. Zhang, X. Wang, and Z. Chen, "Radioactive cobalt(II) removal from aqueous solutions using a reusable nanocomposite: kinetic, isotherms, and mechanistic study," *International Journal of Environmental Research and Public Health*, vol. 14, no. 12, p. 1453, 2017.

[43] S. Hashemian, H. Saffari, and S. Ragabion, "Adsorption of cobalt(II) from aqueous solutions by Fe_3O_4/bentonite nanocomposite," *Water, air, & Soil Pollution*, vol. 226, p. 2212, 2015.

[44] M. Ferri, S. Campisi, and A. Gervasini, "Nickel and cobalt adsorption on hydroxyapatite: a study for the de-metalation of electronic industrial wastewaters," *Adsorption*, vol. 25, no. 3, pp. 649–660, 2019.